Molecular Dynamics Simulations of Nucleic Acids with a Generalized Born Solvation Model

Vickie Tsui and David A. Case*

Contribution from the Department of Molecular Biology, The Scripps Research Institute, La Jolla, California 92037

Received November 8, 1999. Revised Manuscript Received January 13, 2000

Abstract: A generalized Born (GB) model has been applied to molecular dynamics simulations of the A- and B-forms of a duplex DNA d(CCAACGTTGG)$_2$ and the corresponding duplex RNA r(CCAACGUUGG)$_2$, resulting in good agreement with simulations using explicit water solvent in terms of both structure and energetics. In particular, the A → B energy differences derived from GB trajectories for both DNA and RNA closely match those obtained earlier using explicit water simulations and finite-difference Poisson−Boltzmann calculations. A GB simulation starting from A-form DNA converges to B-DNA within 20 ps, more than 20 times faster than the transition from A- to B-DNA in explicit solvent simulations. For B-form d(CCAACGTTGG)$_2$, fluctuations about the mean are highly correlated between GB and explicit water simulations, being slightly larger in the former, and the essential subspaces found from principal component analysis overlap to a high degree. Hence, for many purposes this parametrization offers an alternative to more expensive explicit water simulations for studies of nucleic acid energetics and structure.

1. Introduction

Studies of nucleic acids using molecular dynamics simulations have shown considerable progress during the past five years.[1,2] With the use of particle-mesh Ewald to treat long-range electrostatics, stable trajectories of DNA and RNA molecules up to several nanoseconds have been obtained.[3−12] Details of the structural and dynamical properties of various nucleic acids, ranging from conventional DNA and RNA duplexes to DNA:RNA hybrids, triplex nucleic acids, and RNA hairpin loops, can be elucidated through these MD studies.

To accurately represent the environment, such simulations generally are carried out in the presence of explicit solvent molecules. The box of solvent molecules must be large enough to minimize electrostatic interactions between periodic images of the solute, generally leaving at least 10 Å between each edge of the box and the closest solute atom. This results in a system of around 3000 water molecules for a 10-base pair duplex DNA.[13] In addition to increasing calculation time, complications also arise from the need to fully equilibrate these molecules and any counterions in the system. Even with today's powerful computational facilities, these simulations can be lengthy and costly.

The electrostatic effects of a solvent of high dielectric, such as water, can be approximated by a continuum electrostatics model.[14−16] This model has been extensively studied, mostly through numerical solutions of electrostatic equation in a multiple dielectric model. The generalized Born (GB) model[17−19] provides an approximate solution to the solute−solvent electrostatic polarization term (ΔG_{pol}). This model is often able to reproduce the solvation energies given by the Poisson−Boltzmann (PB) continuum solvent model for a variety of biomolecules, without the costly computations of the numerical solutions to Poisson's equation.[20−28] Furthermore, an extension to the GB model to account for salt effects in the linearized

(1) Leontis, N. B.; SantaLucia, J., Eds., In *Molecular Modeling of Nucleic Acids*; American Chemical Society: Washington, DC, 1998.
(2) Auffinger, P.; Westhof, E. *Curr. Opin. Struct. Biol.* **1998**, *8*, 227−236.
(3) Cheatham, T. E., III; Miller, J. L.; Fox, T.; Darden, T. A.; Kollman, P. A. *J. Am. Chem. Soc.* **1995**, *117*, 4193−4194.
(4) York, D. M.; Yang, W.; Lee, H.; Darden, T.; Pedersen, L. G. *J. Am. Chem. Soc.* **1995**, *117*, 5001−5002.
(5) Young, M. A.; Ravishanker, G.; Beveridge, D. L. *Biophys. J.* **1997**, *73*, 2313.
(6) Cheatham, T. E., III; Miller, J. L.; Spector, T. I.; Cieplak, P.; Kollman, P. A. In *Molecular Modeling of Nucleic Acids*; Leontis, N. B., SantaLucia, J. , Eds.; American Chemical Society, Washington, DC, 1998; pp 285−303.
(7) Beveridge, D. L.; Young, M. A.; Sprous, D. In *Molecular Modeling of Nucleic Acids*; Leontis, N. B., SantaLucia, J.. Eds.; American Chemical Society: Washington, DC, 1998; pp 260−284.
(8) MacKerell, A. D., Jr. In *Molecular Modeling of Nucleic Acids*; Leontis, N. B., SantaLucia, J., Eds.; American Chemical Society: Washington, DC, 1998; pp 304−311.
(9) Yang, L.; Pettitt, B. M. *J. Phys. Chem.* **1996**, *100*, 2564−2566.
(10) Feig, M.; Pettitt, B. M. *J. Phys. Chem. B* **1997**, *101*, 7361−7363.
(11) Feig, M.; Pettitt, B. M. *Biophys. J.* **1998**, *75*, 134−149.
(12) Feig, M.; Pettitt, B. M. *Biophys. J.* **1999**, *77*, 1769−1781.
(13) Cheatham, T. E., III; Kollman, P. A. *J. Mol. Biol.* **1996**, *259*, 434−444.
(14) Tomasi, J.; Persico, M. *Chem. Rev.* **1994**, *94*, 2027−2094.
(15) Honig, B.; Sharp, K.; Yang, A.-S. *J. Phys. Chem.* **1993**, *97*, 1101−1109.
(16) Cramer, C. J.; Truhlar, D. G. *Chem. Rev.* **1999**, *99*, 2161−2200.
(17) Constanciel, R.; Contreras, R. *Theor. Chim. Acta* **1984**, *65*, 1.
(18) Still, W. C.; Tempczyk, A.; Hawley, R. C.; Hendrickson, T. *J. Am. Chem. Soc.* **1990**, *112*, 6127−6129.
(19) Schaefer, M.; Karplus, M. *J. Phys. Chem.* **1996**, *100*, 1578−1599.
(20) Qiu, D.; Shenkin, P. S.; Hollinger, F. P.; Still, W. C. *J. Phys. Chem. A* **1997**, *101*, 3005−3014.
(21) Edinger, S. R.; Cortis, C.; Shenkin, P. S.; Friesner, R. A. *J. Phys. Chem. B* **1997**, *101*, 1190−1197.
(22) Srinivasan, J.; Cheatham, T. E., III; Kollman, P.; Case, D. A. *J. Am. Chem. Soc.* **1998**, *120*, 9401−9409.
(23) Srinivasan, J.; Trevathan, M. W.; Beroza, P.; Case, D. A. *Theor. Chem. Acc.* **1999**, *101*, 426−434.
(24) Dominy, B. N.; Brooks, C. L., III *J. Phys. Chem. B* **1999**, *103*, 3765−3773.
(25) Ghosh, A.; Rapp, C. S.; Friesner, R. A. *J. Phys. Chem. B* **1998**, *102*, 10983−10990.
(26) Rapp, C.; Sendrovic; Friesner, R. A. *Proteins* **1999**, *35*, 173−183.

10.1021/ja9939385 CCC: $19.00
Published on Web 03/04/2000

Debye−Huckel approximation has been shown to give good agreement with PB results.[23] Although many early applications of this model considered the energetics of a relatively small number of conformations (such as snapshots from explicit solvent simulations),[22,23,29−32] its use as an effective solvation model for MD simulations is a natural extension of this earlier work, and some studies for peptides, proteins, and nucleic acids have appeared.[24,33,34]

Here we apply the GB model, using a pairwise descreening approximation introduced by Hawkins et al.,[35] to simulations of a 10-base pair duplex of DNA and RNA in A- and B-form helices. The resulting structures show good agreement with corresponding structures from explicit solvent simulations, in both structures and energetics. We also show that unconstrained A-DNA converges to B-DNA within 20 ps of the GB simulation, compared to 500 ps for an explicit solvent simulation.[13] The results provide a parametrization of the GB model that should provide an effective substitute for explicit solvent simulations for many types of investigations of nucleic acid structure.

2. The Generalized Born (GB) Model

The GB model has been discussed extensively in earlier work. The form used here contains a modification that incorporates a Debye−Huckel term to account for salt effects at low salt concentrations:[23]

$$\Delta G_{\mathrm{pol}}^{\mathrm{GB}} = -\frac{1}{2}\left(1 - \frac{e^{-\kappa f_{\mathrm{GB}}}}{\epsilon}\right)\sum_{ij}\frac{q_i q_j}{f_{\mathrm{GB}}} \qquad (1)$$

where q_i and q_j are atomic partial charges, ϵ is the solvent dielectric constant, κ is the Debye−Huckel screening parameter, and the double sum runs over all pairs of atoms. f_{GB} depends on the effective Born radius α_i and the distance r_{ij} between atoms:

$$f_{\mathrm{GB}} = [r_{ij}^2 + \alpha_{ij}^2 \exp(-D_{ij})]^{1/2} \qquad (2)$$

where $\alpha_{ij} = (\alpha_i\alpha_j)^{1/2}$ and $D_{ij} = r_{ij}^2/(2\alpha_{ij})^2$. As $r_{ij} \rightarrow 0$, $f_{\mathrm{GB}} \rightarrow \alpha_i$, the effective radius that establishes the self-energy of charges, which arises from polarization of the surrounding dielectric medium. The f_{GB} function can be thought of as an interpolation formula that reduces to these self-energy terms at short distances, and to a Debye−Huckel screened Coulomb interaction at large distances.

The effective Born radii roughly describe the average distance from a charge to the dielectric boundary, and depend on the positions and volumes of all other atoms in the solute. The original formulation[18] estimated this from a numerical integration procedure, and more recently, several analytical approximations to determining these self-energies (and hence the α_i) have been proposed.[19,20,35] Here we adopt the method of Hawkins, Cramer, and Truhlar,[35,36] which uses a pairwise descreening approximation (PDA) to estimate α_i from a sum over atom pairs:

$$\alpha_i^{-1} = \rho_i^{-1} - \sum_{j\neq i} g(r_i, r_j, \rho_i, \rho_j) \qquad (3)$$

Here ρ_i is an intrinsic radius for atom i, and $g(\,)$ is a positive function, so that the effective radius α_i is greater than the intrinsic radius ρ_i. The function g depends on the positions and sizes of the atoms, but not on their charges. These general characteristics apply not only to the Hawkins et al. model used here,[35,36] but also to related approaches such as ACE,[19] and the "fast analytical" method of Qiu et al.[20,24] For the PDA model used here, the explicit form of $g(\,)$ is given by eq 13 in ref 35; this model, including exact derivatives of all terms, has been incorporated into version 6 of the Amber package,[37] and into version 4 of Nucleic Acid Builder.[38]

The final piece of this prescription for approximate electrostatics is to establish a prescription for the intrinsic radii ρ_i. For each atomic sphere (here characterized by its Bondi radius R_i), the contribution of all other spheres to dielectric screening is calculated from an analytical formula for two (possibly overlapping) spheres. One complication arises from the overestimation of the Born radius, and thus underestimation of G_{pol}, when these neighboring spheres overlap each other. A linear scaling of the R_i values can approximately account for this effect;[35] here the intrinsic radius ρ_i of atom i, used to compute effective Born radii, becomes

$$\rho_i = S_i(R_i + b_{\mathrm{offset}}) \qquad (4)$$

There are clearly many combinations of S_i, R_i, and b_{offset} that could be used. We began with the Bondi set of radii[39] for R_i (based on good experience in earlier numerical Poisson−Boltzmann calculations),[40−44] adopted S_i values from the tinker package[45,46] (shown in Table 1), and made minor adjustments (discussed below) to optimize agreement with finite-difference

Table 1. Optimized Parameters for GB-MD Simulations[a]

atom	R (Å)	S_x	atom	R (Å)	S_x
H^O	0.80	0.85	O	1.50	0.85
H^N	1.20	0.85	N	1.55	0.79
H^C	1.30	0.85	P	1.85	0.86
C	1.70	0.72			

[a] b_{offset} is −0.13 Å (see eq 4).

(27) Jayaram, B.; Liu, Y.; Beveridge, D. L. *J. Phys. Chem.* **1998**, *109*, 1465−1471.
(28) Jayaram, B.; Sprous, D.; Beveridge, D. L. *J. Phys. Chem. B* **1998**, *102*, 9571−9576.
(29) Jayaram, B.; Sprous, D.; Young, M. A.; Beveridge, D. *J. Am. Chem. Soc.* **1998**, *120*, 10629−10633.
(30) Srinivasan, J.; Miller, J.; Kollman, P. A.; Case, D. A. *J. Biomol. Struct. Dyn.* **1998**, *16*, 671−682.
(31) Wagner, F.; Simonson, T. *J. Comput. Chem.* **1999**, *20*, 322−335.
(32) Vorobjev, Y. N.; Almagro, J. C.; Hermans, J. *Proteins* **1998**, *32*, 399−413.
(33) Schaefer, M.; Bartels, C.; Karplus, M. *J. Mol. Biol.* **1998**, *284*, 835.
(34) Williams, D. J.; Hall, K. B. *Biophys. J.* **1999**, *76*, 3192−3205.
(35) Hawkins, G. D.; Cramer, C. J.; Truhlar, D. G. *Chem. Phys. Lett.* **1995**, *246*, 122−129.
(36) Hawkins, G. D.; Cramer, C. J.; Truhlar, D. G. *J. Phys. Chem.* **1996**, *100*, 19824−19839.
(37) Case, D. A.; Pearlman, D. A.; Caldwell, J. C., III; Cheatham, T. E.; Ross, W. S.; Simmerling, C. L.; Darden, T. A.; Merz, K. M.; Stanton, R. V.; Cheng, A. L.; Vincent, J. J.; Crowley, M.; Tsui, V.; Radmer, R. J.; Duan, Y.; Pitera, J.; Massova, I.; Seibel, G. L.; Singh, U. C.; Weiner, P. K.; Kollman, P. A., *AMBER 6*; University of California: San Francisco 1999.
(38) Macke, T. J.; Case, D. A. In *Molecular Modeling of Nucleic Acids*; Leontis, N. B., SantaLucia, J., Eds.; Washington, DC, 1998; pp 379−393.
(39) Bondi, A. *J. Chem. Phys.* **1964**, *64*, 441.
(40) Ösapay, K.; Young, W.; Bashford, D.; Brooks, C. L., III; Case, D. A. *J. Phys. Chem.* **1996**, *100*, 2698−2705.
(41) Bashford, D.; Case, D. A.; Dalvit, C.; Tennant, L.; Wright, P. E. *Biochemistry* **1993**, *32*, 8045−8056.
(42) Chen, J. L.; Noodleman, L.; Case, D. A.; Bashford, D. *J. Phys. Chem.* **1994**, *98*, 11059−11068.
(43) Richardson, W. H.; Peng, C.; Bashford, D.; Noodleman, L.; Case, D. A. *Int. J. Quantum Chem.* **1997**, *61*, 207−217.
(44) Demchuk, E.; Bashford, D.; Gippert, G.; Case, D. A. *J. Mol. Biol.* **1997**, *270*, 305−317.
(45) Dudek, M. J.; Ponder, J. W. *J. Computat. Chem.* **1995**, *16*, 791−816.
(46) http://dasher.wustl.edu/tinker 1995.

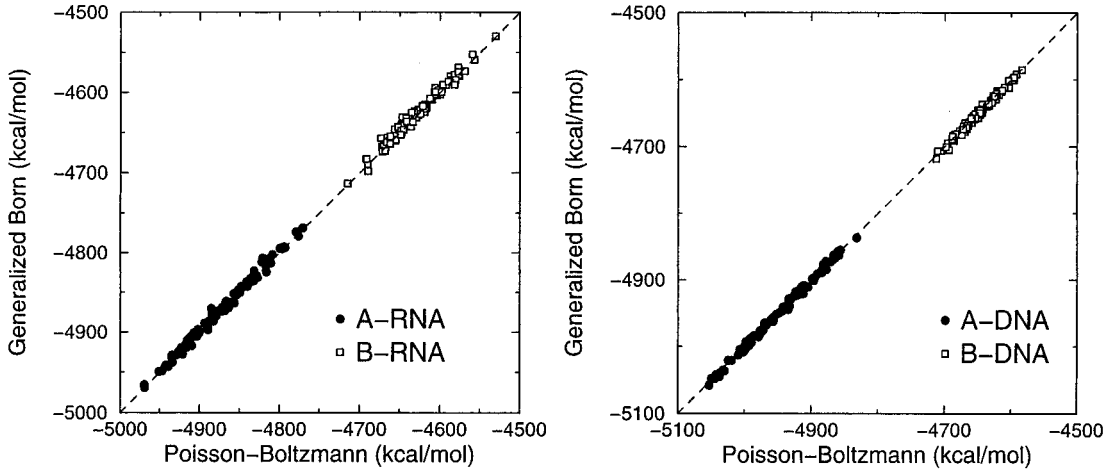

Figure 1. Plot of GB vs PB energies. Details on the calculation of these energy terms are described in the Appendix. Energies are plotted for 100 snapshots from each of the following explicit solvent simulations: A-RNA and B-RNA (left), A-DNA and B-DNA (right).

Poisson−Boltzmann calculations. The resulting parameters are shown in Table 1.

The linearized Debye−Huckel approximation used here in conjunction with GB has been shown to successfully reproduce the salt dependence of Poisson−Boltzmann calculations. The Debye−Huckel screening parameter κ in eq 1 is multiplied by 0.73 to account for the overestimation of salt effects, as described earlier.[23] Addition of salt contribution to the GB simulations did not affect the structures greatly; out of the parameters examined below, the most prominent improvement came in the *x*-displacement, whose average shifted toward the explicit solvent values by about 0.5 Å in both the A-RNA and B-DNA simulations upon adding 0.2 M salt. (Structures carried out with either 0.1 or 0.2 M salt concentrations were almost identical.) Because of minor shifts of the *x*-displacement and inclination parameters toward explicit solvent values, the GB simulations in this study were performed at 0.2 M salt concentration, with a solvent dielectric of 78.5 and a solute dielectric of unity. The explicit water results were taken from published work, and the GB simulations carried in a standard fashion; full details are given in the Appendix.

3. Results and Discussion

3.1. Adjustment of Parameters. In our earlier studies applying the generalized Born model to snapshots from explicit water simulations,[22] we had used the PARSE radii set of Sitkoff et al.[47] to define the dielectric boundary between solute and solvent, along with the original value of b_{offset} of −0.09 Å, suggested by Still et al.[18] These parameters gave good results for the energy difference between B- and A-form helices, but preliminary MD simulations of B-DNA resulted in dissociation of the two strands within 100 ps. We hypothesized that this might arise from too great a weakening of the Watson−Crick hydrogen bonds due to solvent screening, and attempted a second round of simulations, increasing the hydrogen atom radius from its value of 1.0 Å in the PARSE set to the value of 1.2 Å that appears in the Bondi radii.[39] (This is one of the largest differences between the PARSE and Bondi radii sets.) This change in radii produced stable trajectories of double-stranded nucleic acids. The relative GB energies between various conformations of the 10-base pair DNA matched those of PB calculations fairly well; however, those of the RNA were less successful in reproducing the PB results. An analysis of the individual energy terms in the two simulations pointed to the 2′-hydroxyl hydrogen atoms of the RNA. We thus treated the hydrogen atoms as three different groups based on their covalently bonded partners: the hydroxyl hydrogens, the amino hydrogens, and the aliphatic hydrogens. Upon optimization of these hydrogen radii against relative PB energies for various conformations of DNA and RNA, we arrived at 0.8 Å for hydroxyl hydrogens, 1.2 Å for hydrogens bonded to nitrogen, and 1.3 Å for hydrogens bonded to carbon. The order of sizes is reasonable considering the electronegativities of their bonding partners, and matches the order of hydrogen sizes used in the Cornell et al. force field being used for the gas-phase portion of our energy function (i.e. HC > HN > HO).[48] Adjustment of b_{offset} to −0.13 Å allowed the absolute GB energies to reproduce those of PB for a variety of RNA and DNA conformations, taken from snapshots of the explicit solvent simulations (Figure 1). For the 200 RNA structures analyzed, the correlation coefficient and rms error between GB and PB energies were 0.999 and 5.029 kcal/mol, respectively. For the 200 DNA structures analyzed, the correlation coefficient and rms error between GB and PB energies were 0.999 and 3.884 kcal/mol, respectively. The final parameters used are summarized in Table 1. While it is clear that other combinations of parameters might also work well, this set has the advantage of simplicity, using the well-established Bondi radii, modified only to make hydrogen atoms bonded to carbon slightly larger and hydrogens bonded to oxygen slightly smaller.

3.2. Comparison between GB and Explicit Solvent Simulations. 3.2.1. Average Structures. The GB simulations remained stable throughout the 2 ns simulation time, as can be seen in the heavy-atom RMSD plot of the A-RNA and B-DNA trajectories from the mean structure of the simulations (Figure 2). This also shows that the fluctuations of the GB structures about their own mean (solid lines) are nearly the same as the deviations from the mean of the explicit water simulation (dashed lines). Tables 2 and 3 compare the mean structures from the GB and water simulations to each other and to "canonical" helical structures derived from fiber diffraction. The RMSDs between the GB and explicit solvent simulations are 1.00 Å for A-RNA and 0.88 Å for B-DNA, calculated for the inner eight base-pairs. The RMSDs are larger between GB and explicit solvent B-RNA (1.14 Å) and A-DNA (1.78 Å), most probably

(47) Sitkoff, D.; Sharp, K. A.; Honig, B. *J. Phys. Chem.* **1994**, *98*, 1978−1988.

(48) Cornell, W. D.; Cieplak, P.; Bayly, C. I.; Gould, I. R.; Merz, K. M., Jr.; Ferguson, D. M.; Spellmeyer, D. C.; Fox, T.; Caldwell, J. W.; Kollman, P. A. *J. Am. Chem. Soc.* **1995**, *117*, 5179−5197.

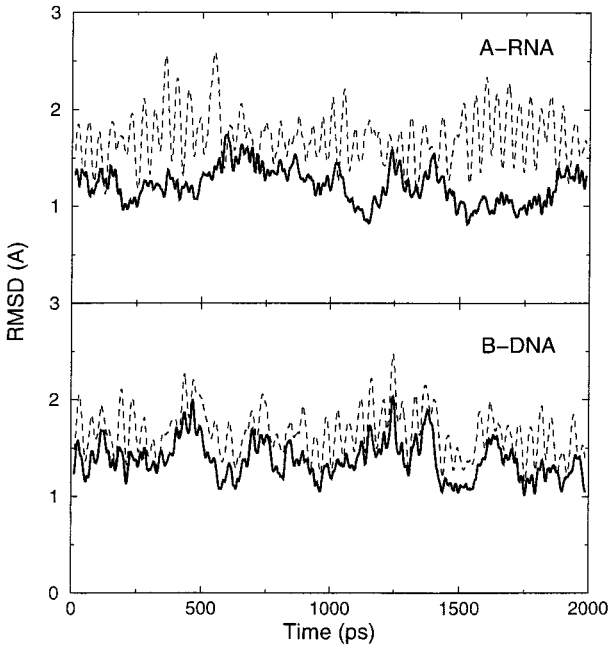

Figure 2. Root-mean-square deviation (RMSD) over the course of the 10-base pair A-RNA (top) and B-DNA (bottom) GB simulations. RMSDs were calculated for all residues with respect to the mean structures of the respective GB simulations (solid line) as well as to the mean structures of the respective explicit solvent simulations (dashed line). The data have been smoothed by performing a running average over 25 ps.

because of the different methods used to maintain the nucleic acids in these less favorable conformations: artificial sugar-pucker restraints were used for the GB simulations (see the Appendix), whereas a mixed alcohol−water solvent environment was used for the explicit simulations. Although each simulation method evolves to its own average structure, overall the values support the use of the "A" and "B" nomenclature for the various structures.

This conclusion is further justified by the results in Figures 3 and 4, which compare selected helical parameters for B-DNA and A-RNA. Although there are large fluctuations about the means in all of the simulations, the averages shown in circles exhibit similar trends for GB and explicit water, especially in the rise and twist parameters. For B-DNA (Figure 3), the rise between base pairs adopts the same pattern in both simulations, with higher rise in the center and the two ends of the DNA. The high twist values in the center of the explicit solvent structures, however, are not observed in the GB structures. Upon examination of the explicit solvent trajectory, the high average twist at steps C5-G6 to G6-T7 arises partly from the high twist in the first 200 ps, where it has an average twist of ∼40°. Otherwise the mean helical parameters for GB B-DNA are nearly identical with those from the explicit water simulations.

This correlation of relative helical parameters between base pairs is even more evident when comparing GB and explicit solvent structures of A-RNA (Figure 4). The GB simulations do, however, lead to structures with slightly higher values of rise between base pairs and lower values of helical twist; again, the pattern along the sequence (e.g. with low inclination in the middle) is the same for both methods. The sugar pucker pseudorotation angles of the GB structures replicate those of explicit solvent structure, with the exception of a few end nucleotides. The residue 10 sugar ring in the explicit solvent simulation switches back and forth between C3′-endo and C2′-endo conformations; in the GB simulation, this sugar pucker remains in the C2′-endo conformation throughout the trajectory. Comparing the pseudorotation angles of A-RNA with B-DNA, we also see that the range of the sugar conformations adopted is smaller in A-RNA than in B-DNA. In both GB and explicit solvent simulations, the B-DNA sugars occasionally sample the northeast conformations, while the A-RNA sugars generally remain in the north to northeast conformations. In addition, the crankshaft (α, γ: g−,g+ to t,t) transition observed in the explicit solvent simulation at the CpG step was retained in the GB simulation of this A-RNA sequence while the other steps maintained the gauche−, gauche+ conformations, consistent in both simulations of the A-RNA (data not shown).

3.2.2. Fluctuations about the Mean. In comparing MD results from different solvation models, it is instructive to look not only at the average structures, but also at fluctuations about the mean. Figure 5 plots RMS fluctuations about the mean for each atom in the central eight base pairs of B-form d(C-CAACGTTGG)$_2$. It is clear that there is a very high correlation between the two simulation methods, with the mean fluctuation being slightly higher (1.23 Å vs 1.15 Å) in the GB model. The same trend is seen in the A-RNA simulations where the average fluctuation for atoms in the central eight base pairs is 1.11 Å for GB and 0.96 Å for explicit solvent. Both GB and explicit solvent simulations show A-RNA to be slightly more rigid than B-DNA, in accord with previous simulations and with the expected consequence of the extra steric bulk of the 2′-hydroxyl group.

Fluctuations can also be compared to performing a quasi-harmonic or principal component analysis, obtained by diagonalizing the second-moment matrix of fluctuations about the mean, as described in the Appendix.[49,50] Figure 6 shows a close agreement between the quasiharmonic frequency distributions derived from GB and from explicit water simulations. As is well-known, most of the fluctuation amplitude arises from a fairly small number of "essential" modes.[49−51] Figure 7 shows the overlap of the five highest amplitude modes from the explicit water simulation, with subspaces derived from various numbers of modes from the GB simulation. Each of the water modes overlaps to greater than 0.8 with a subspace formed from the first 40 GB modes. This is similar to the behavior that would be seen from independent simulations in the same force field,[52] and supports the notion that the nature of fluctuations seen for the GB simulation has a character very similar to that from the explicit water reference simulation.

Similar conclusions can be drawn from the analysis of helical parameters shown in Figures 3 and 4. In general, the standard deviations, especially those of the *x*-displacement, are modestly higher in the GB structures. This observation is correlated with the increased fluctuations in the implicit solvent model. The end base pairs of B-DNA have the largest standard deviations, as expected. In fact, openings of the end base pairs were observed occasionally in the GB B-DNA simulation, although these disruptions were transient, and the base-pairs would soon reform their Watson−Crick hydrogen bonds. Many fewer excursions of this sort were seen in the explicit water simulation.

3.2.3. Energies. To compare the relative energetic contributions between the B-form and A-form of RNA and DNA, GB simulations of B-RNA and A-DNA were carried out with

(49) Karplus, M.; Kushick, J. N. *Macromolecules* **1981**, *14*, 325−332.
(50) Amadei, A.; Linssen, A. B. M.; Berendsen, H. J. C. *Proteins* **1993**, *17*, 412−425.
(51) Case, D. A. *Curr. Opin. Struct. Biol.* **1994**, *4*, 285−290.
(52) Amadei, A.; Ceruso, M. A.; Di Nola, A. *Proteins* **1999**, *36*, 419−435.

Table 2. Structural Comparisons for d(CCAACGTTGG)$_2$[a,b]

	A-DNA	B-DNA	AD_wat	BD_wat	AD_GB	BD_GB
A-DNA		5.46	1.50	3.81	2.10	3.73
B-DNA	4.54		5.18	2.75	4.19	3.31
AD_wat	1.31	4.37		3.69	1.98	3.72
BD_wat	3.46	2.15	3.37		2.16	0.93
AD_GB	1.71	3.43	1.78	2.09		2.33
BD_GB	3.29	2.71	3.34	0.88	2.10	

A-DNA: Canonical A-DNA generated by nucgen, a module of AMBER 6
B-DNA: Canonical B-DNA generated by nucgen, a module of AMBER 6
AD_wat: Mean structure of 100 snapshots of explicit solvent simulation of A-DNA at 10 ps intervals
BD_wat: Mean structure of 100 snapshots of explicit solvent simulation of B-DNA at 10 ps intervals
AD_GB: Mean structure of 100 snapshots of GB simulation of A-DNA at 10 ps intervals
BD_GB: Mean structure of 100 snapshots of GB simulation of B-DNA at 10 ps intervals

[a] Shown are heavy-atom root-mean-square deviations (haRMSD) between the specified structures. [b] The upper triangle represents haRMSD fit (in Å) calculated for all nucleotides. The lower triangle represents haRMSD fit calculated for the internal 8 base pairs d(CAACGTTG)$_2$, i.e., residues 2 to 9 and 12 to 19.

Table 3. Structural Comparisons for r(CCAACGUUGG)$_2$[a]

	A-RNA	B-RNA	AR_wat	BR_wat	AR_GB	BR_GB
A-RNA		5.16	1.82	3.44	2.48	4.32
B-RNA	4.33		4.90	3.19	5.56	2.41
AR_wat	1.84	3.95		2.62	1.22	3.62
BR_wat	3.26	2.59	2.33		3.06	1.49
AR_GB	2.38	4.58	1.00	2.76		3.96
BR_GB	3.85	2.08	2.96	1.14	3.34	

A-RNA: Canonical A-RNA generated by nucgen, a module of AMBER 6
B-RNA: Canonical B-RNA generated by nucgen and leap, modules of AMBER 6
AR_wat: Mean structure of 100 snapshots of explicit solvent simulation of A-RNA at 10 ps intervals
BR_wat: Mean structure of 100 snapshots of explicit solvent simulation of B-RNA at 10 ps intervals
AR_GB: Mean structure of 100 snapshots of GB simulation of A-RNA at 10 ps intervals
BR_GB: Mean structure of 100 snapshots of GB simulation of B-RNA at 10 ps intervals

[a] See captions for Table 2.

structural restraints. Unlike explicit solvent simulations, B-RNA did not remain stable in the simulation time; instead, the bases became distorted and lost Watson−Crick interactions, while the sugar pucker stayed in the south conformation. The overall energies of these distorted conformations are higher than those of A-RNA conformations, indicating that the structures were trapped in the midst of adjusting away from the B-form conformations. With the addition of structural restraints as described in the Appendix, the B-RNA and A-DNA simulations produced stable trajectories with helical parameters comparable to those of explicit solvent simulations (data not shown).

Tables 4 and 5 list the average energy terms for the simulations along with their standard deviations. The explicit solvent structures are the same as the ones analyzed by Srinivasan et al., and the average internal energy, van der Waals energy, and Coulomb energy terms were published previously.[22] The GB energies were re-computed for these explicit solvent structures using the set of parameters described above, with 0.2 M salt concentration. Here the hydrophobic energy, which can be approximated by a term proportional to the solvent-accessible surface area,[20,35,47] is excluded from these energy analyses as well as from the GB MD simulations. Previous studies found that the A- versus B-form duplex DNA and RNA have very similar surface areas, such that the hydrophobic term has negligible contributions to the relative conformational energies.[22] This may not be true for more drastic conformational changes, such as those involved in strand separation, and we cannot predict from the present results how well our models would work for such large conformational changes. The ability to carry out molecular dynamics simulations using a combined GB/SA (surface area) model has been implemented in version 6 of Amber,[37] and further studies on the effects of the hydrophobic term on various systems will be published elsewhere.

As can be seen in Tables 4 and 5, the individual terms as well as the relative (B−A) energies compare well between GB and explicit solvent structures. The gas-phase Coulomb interaction energy $\langle E_{elec} \rangle$ is known to be strongly anti-correlated with the electrostatic solvation term $\langle E_{GB} \rangle$, such that the total electrostatic energies $\langle E_{elec\_tot} \rangle$ are closely matched between GB and explicit solvent structures. The $\langle E_{tot} \rangle$ values for both GB and explicit solvent favor A-form helices for RNA and B-form helices for DNA; a detailed analysis of these differences has been presented earlier.[22] The internal energies of B-RNA and A-DNA are higher in GB than in the explicit solvent simulations. This could be due to the structural constraints leading to adjustments to satisfy these constraints while making sacrifices in the internal energies. These may also be structural adjustments made to lower the van der Waals energy while causing increase in the internal energy, as can be seen in the van der Waals energy terms of B-RNA and A-DNA.

3.3. Transition from A-DNA to B-DNA. In addition to the A-DNA simulation performed with distance and torsion angle restraints, we also carried out GB simulations starting with A-DNA without any structural restraints. Using explicit solvent MD with PME, unconstrained A-form DNA was shown to converge to B-form within 500 ps.[13] Because of the increased mobility in GB simulations, in which the solute is free to move without any readjustment of water structures, we set out to test if A-DNA would convert to B-DNA at a faster rate using GB with MD simulations.

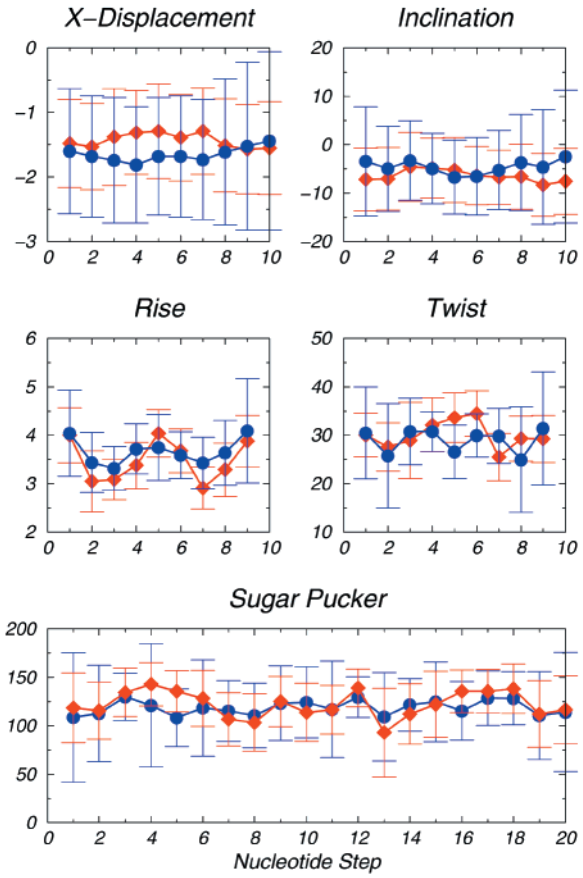

Figure 3. Plots of *x*-displacement, inclination, rise between base pairs (rise), helical twist (twist), and sugar pucker vs nucleotide step for the GB (blue circle) and explicit solvent (red diamond) simulations of the B-DNA d(CCAACGTTGG)$_2$. Average values and standard deviations and standard deviations are plotted for 100 snapshots taken at 10 ps intervals for the last nanosecond of the trajectory. The values are presented traversing the helix from the 5′ to 3′ direction, i.e., residue 11 represents the 5′ end of the second strand (C11). *x*-displacement and rise are expressed in Å; inclination, helical twist and sugar pucker are expressed in degrees.

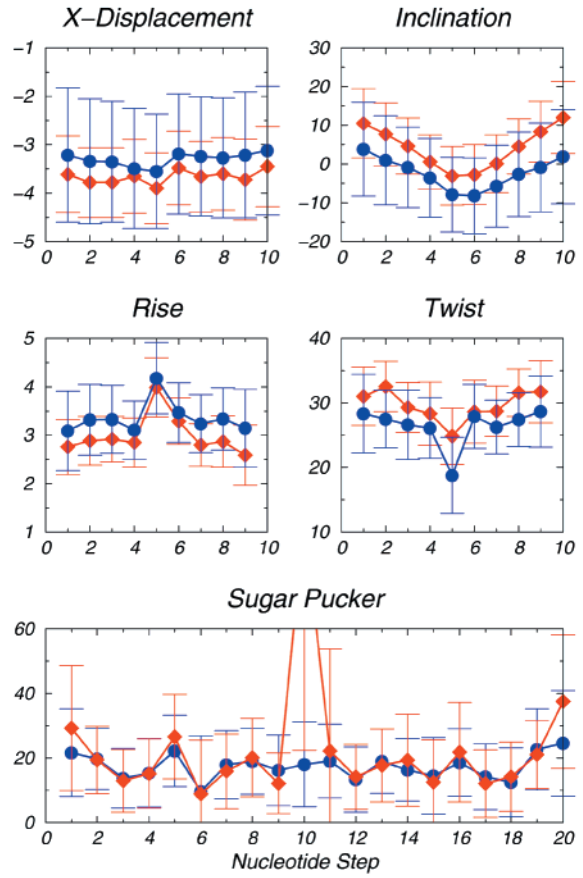

Figure 4. Plots of *x*-displacement, inclination, rise between base pairs (rise), helical twist (twist), and sugar pucker vs nucleotide step for the GB (blue circle) and explicit solvent (red diamond) simulations of the A-RNA r(CCAACGUUGG)$_2$. See Figure 3 for explanations of parameters.

Figure 8 shows the propagation of average sugar pucker and minor groove width for the first 50 ps of the trajectory, starting at the beginning of the simulation without harmonic constraints. Within 5 ps after the harmonic constraints are turned off, the sugar pucker has already converged with the simulation starting with B-DNA. The quick transition can also be seen in the rapid decrease of the minor groove width from a value close to the canonical A-form minor groove width (18.8 Å) to the width of the B-DNA simulation. This speed of transition is more than 20 times faster than the transition seen in explicit solvent simulations, in which both the average sugar pucker and the minor groove width took 500 ps to reach the B-form values using the same 10-base pair sequence.

The process of this transition is represented in Figure 9 as four snapshots from the first 20 ps of the trajectory, starting with a structure close to the canonical A-form DNA (0.46 Å RMSD for all residues). At 5 ps, the change in the structure is already obvious, with a decrease in the minor groove width accompanied by an opening of the major groove. The structure is further stretched out to adjust itself. It adopts a somewhat distorted structure at 10 ps, but is quickly relaxed to the well-converged structure at 20 ps, which remains stable for the remainder of the 1 ns simulation. The structure at 20 ps has an end-to-end length of 31.6 Å, close to the length of the canonical B-form (30.4 Å) and stretched out from the 25.4 Å long A-form

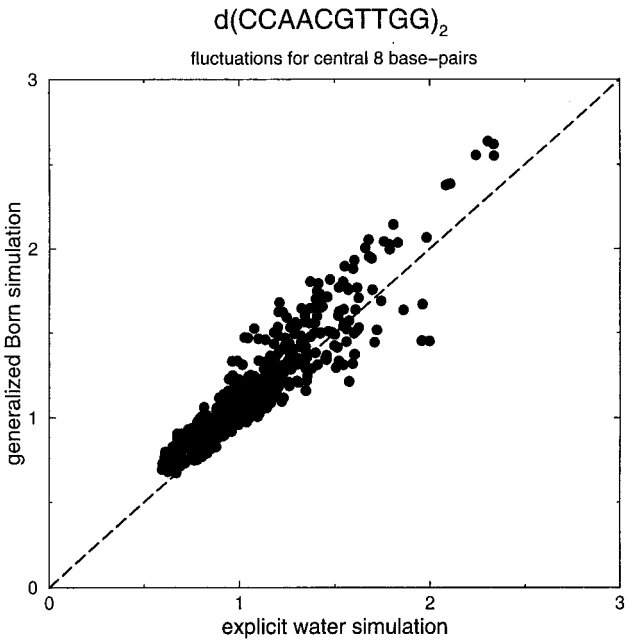

Figure 5. Atomic fluctuations of the central 8 base pairs of d(CCAACGTTGG)$_2$ about the mean. Fluctuations of each atom computed from the generalized Born simulation are plotted against fluctuations computed from the explicit water simulation.

structure at 0 ps. The mean structure of the 1 ns simulation has only a 0.38 Å all-residue RMSD from the mean structure of the GB simulation starting from B-DNA, illustrating the ability

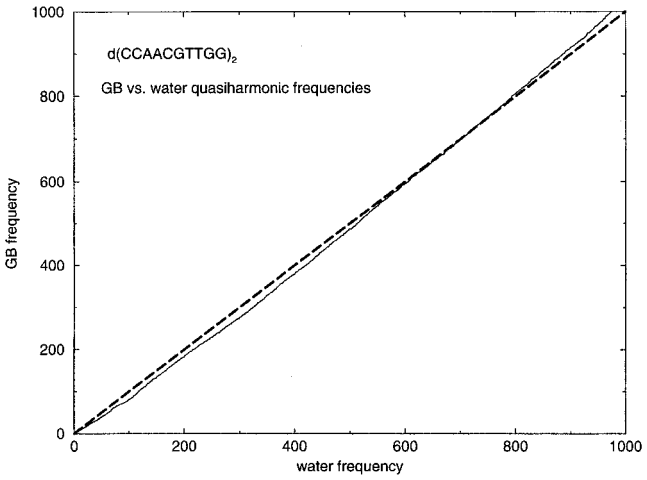

Figure 6. Plot of frequencies of quasiharmonic modes calculated from the GB simulation of d(CCAACGTTGG)$_2$ versus those calculated from the explicit solvent simulation, for the lowest 1077 modes with frequencies below 1000 cm^{-1} (solid line). The dotted line indicates the ideal case of identical frequencies.

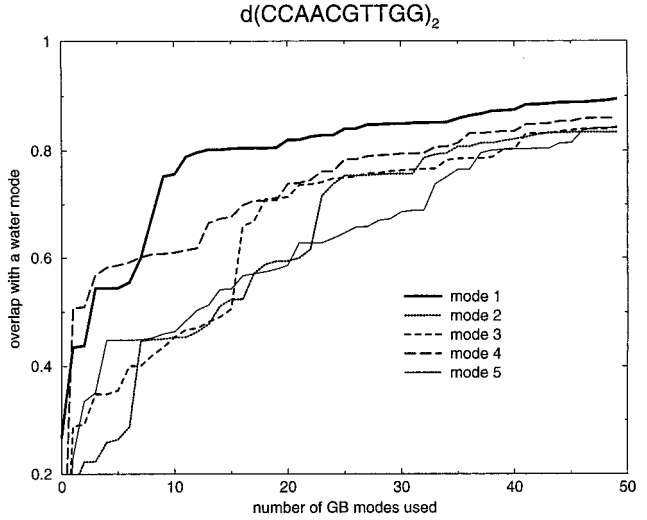

Figure 7. Plot of the overlap of each of the first five quasiharmonic modes calculated from the explicit solvent simulation of d(CCAACGTTGG)$_2$ with modes calculated from the GB simulation. The overlap is computed as the cumulative inner products of the specified water eigenvector with the GB eigenvectors, and it is plotted as a function of the number of GB modes used in the calculation.

of GB to produce rapidly convergent structures starting from different conformations.

This accelerated transtion from A to B is most likely due to the lack of solvent frictional effects in the GB model. This is both an advantage (in that conformational transitions and equilibration can take place more rapidly) and a disadvantage (in that the time dependence of dynamical behavior is incorrect). We are exploring the use of Langevin equations in conjunction with the GB model for studies where a more correct dynamical description is required.

3.4. Performance. The simulations used Amber version 6 on a Cray T3E-900 computer. Table 6 lists the performance results of 0.1 ps simulations of the 10-base pair B-form DNA, d(CCAACGTTGG)$_2$, using vacuum, generalized Born, and explicit water models. Both the vacuum and generalized Born simulations were carried out with a 1 fs time step and 15 Å cutoff. The explicit solvent simulation used a 1 fs time step with a 9 Å nonbonded cutoff for the direct-space interactions, and the PME method for the reciprocal space portion. Timings are reported for simulations carried out with 2, 4, 8, and 16 processors. The efficiency, calculated here as

$$\text{efficiency} = \frac{(\text{time using 2 processors}) \times 2}{(\text{time using } n_{\text{proc}}) \times n_{\text{proc}}} \qquad (5)$$

is also reported for the various runs. Generalized Born simulations are approximately 5 times slower than vacuum simulations and 7 times faster than explicit solvent simulations. As can be seen in Table 6, these GB simulations are efficiently parallelized. This speedup will allow studies of longer pieces of nucleic acids within a reasonable simulation time, and will expand the abilities of MD simulations to produce longer trajectories of larger molecules.

4. Conclusions

We report here the results from 2 ns MD simulations of a 10-base pair B-DNA, A-RNA, A-DNA, and B-RNA, using the generalized Born (GB) model to approximate the electrostatic contribution to the free energy of solvation. Using the GB parameters presented in Table 1, optimized to give close agreement with finite-difference Poisson−Boltzmann calculations (Figure 1), the pairwise descreening approximation to the GB model[35] resulted in stable trajectories whose structures, fluctuations, and energetics are quite similar to those seen in parallel explicit solvent simulations.

It is worth noting that it is not trivial to obtain such behavior. In addition to the GB simulations described above (where strand dissociation was seen with smaller hydrogen radii), we also performed a variety of vacuum simulations on the 10-base pair B-form DNA, d(CCAACGTTGG)$_2$. As described in the Appendix, simulations were carried out with distance dependent dielectric function (*ddd*) as well as a constant dielectric of 78.5. Both structures resulted in distorted DNA. The *ddd* structures were characterized by narrow minor grooves, very low inclination, and high twist. The constant dielectric structures at first dissociated into single strands. After adding hydrogen bond distance restraints, the strands stayed together but the helix was mostly unwound. It is conceivable that adjusting the force field of the nucleic acid could lead to a stable helical trajectory in an alternate environment (constant dielectric or *ddd*). However, using the well-established Cornell et al. force field[48] (which has been shown to produce numerous successful PME simulations),[3,13,53] these results show that the generalized Born solvation term plays an important role in driving the nucleic acid toward reasonable structures. It is known that even explicit solvation simulations of duplex nucleic acids are sensitive to conditions of the simulations (such as how long-range electrostatic interactions are treated),[6−8] so that the present results represent an impressive first test for the use of the GB model to account for solvation effects in MD simulations.

The GB simulations produced stable trajectories, resulting in structures that matched well with corresponding structures from explicit solvent simulations. Some small systematic deviations were observed for both the DNA and the RNA, such as higher rise between base pairs and lower helical twist values of the GB structures, and these deviations could represent the structural properties most sensitive to the effects of interactions with explicit water molecules. The energy terms of the 10-base pair DNA and RNA structures from GB simulations compared well to the energies calculated from explicit solvent structures,

(53) Cheatham, T. E., III; Kollman, P. A. *J. Am. Chem. Soc.* **1997**, *119*, 4805−4825.

Table 4. Energy Terms[a] for d(CCAACGTTGG)$_2$[b]

	B-DNA		A-DNA		B−A	
	GB	WAT	GB	WAT	GB	WAT
⟨*E*(int)⟩	859.0 ± 15.1	860.5 ± 19.2	895.1 ± 15.1	867.5 ± 16.9	−36.1	−7.0
⟨*E*(vdw)⟩	−172.3 ± 9.2	−166.8 ± 8.5	−183.3 ± 7.7	−159.1 ± 8.7	11.0	−7.7
⟨*E*(elec)⟩	−140.0 ± 41.5	−88.9 ± 33.1	92.4 ± 42.9	204.4 ± 56.8	−232.4	−293.3
⟨*E*(GB)⟩	−4633.4 ± 37.6	−4688.4 ± 29.2	−4866.8 ± 40.4	−4979.2 ± 54.9	233.4	290.8
⟨*E*(elec_tot)⟩	−4773.4 ± 10.1	−4777.3 ± 9.0	−4774.4 ± 9.7	−4774.8 ± 8.6	1.0	−2.5
⟨*E*(tot)⟩	−4086.7 ± 12.6	−4083.6 ± 17.9	−4062.6 ± 12.6	−4066.4 ± 16.9	−24.1	−19.7

[a] Energies were calculated from 100 structures in each of the GB and WAT simulations. Average and standard deviation are reported in kcal/mol. [b] ⟨*E*(int)⟩, internal energy. ⟨*E*(vdw)⟩, van der Waals energy. ⟨E(elec)⟩, Coulomb energy. ⟨*E*(GB)⟩, generalized Born. ⟨*E*(elec_tot)⟩, *E*(elec) + *E*(GB). ⟨*E*(tot)⟩, *E*(int) + *E*(vdw) + *E*(elec) + *E*(GB).

Table 5. Energy Terms[a] for r(CCAACGUUGG)$_2$[b]

	B-RNA		A-RNA		B−A	
	GB	WAT	GB	WAT	GB	WAT
⟨*E*(int)⟩	959.7 ± 15.4	944.0 ± 17.8	926.4 ± 15.2	926.4 ± 19.0	33.3	17.6
⟨*E*(vdw)⟩	−174.4 ± 9.0	−149.4 ± 11.3	−182.7 ± 9.0	−168.1 ± 9.3	8.3	18.7
⟨*E*(elec)⟩	−270.0 ± 42.3	−333.4 ± 37.1	−96.5 ± 43.7	−66.5 ± 50.4	−173.5	−266.9
⟨*E*(GB)⟩	−4723.2 ± 38.5	−4658.8 ± 33.2	−4875.4 ± 40.2	−4908.3 ± 45.3	152.2	249.5
⟨*E*(elec_tot)⟩	−4993.2 ± 9.8	−4992.2 ± 10.8	−4971.9 ± 9.9	−4974.8 ± 9.4	−21.3	−17.4
⟨*E*(tot)⟩	−4207.9 ± 12.4	−4197.6 ± 17.4	−4228.2 ± 12.3	−4216.5 ± 18.1	20.3	18.9

[a] See caption for Table 4. [b] ⟨*E*(int)⟩, internal energy. ⟨*E*(vdw)⟩, van der Waals energy. ⟨E(elec)⟩, Coulomb energy. ⟨*E*(GB)⟩, generalized Born. ⟨*E*(elec_tot)⟩, *E*(elec) + *E*(GB). ⟨*E*(tot)⟩, *E*(int) + *E*(vdw) + *E*(elec) + *E*(GB).

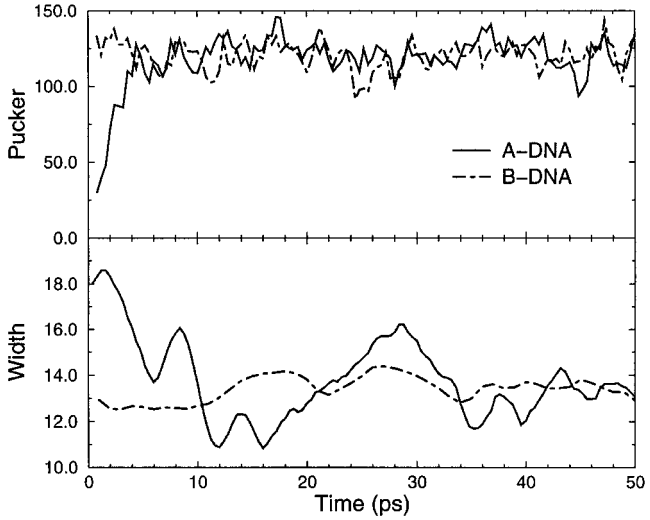

Figure 8. Plots of average sugar pucker (pucker) and minor groove width (width) over the course of the GB simulations starting from A-DNA and B-DNA. The sugar pucker at each snapshot is averaged over all residues. The minor groove width at each snapshot is averaged over the following inter-strand phosphate distances: C5-G20, G6-G19, T7-T18, T8-T17, G9-G16, and G10-C15.

giving relative energies between A- and B-form helices similar to those of explicit solvent simulations.

The unconstrained simulation of A-DNA converged to B-DNA within 20 ps using GB. This is more than 20 times faster than the transition of A- to B-DNA in explicit solvent, which took ∼500 ps without special sampling techniques. This rapid convergence is correlated with the overall increase in mobility of GB simulations relative to explicit solvent simulations, and is most probably because of the lack of frictional forces introduced by the water molecules, and the lack of a need for re-organization of water molecules to balance changes in solute structure. This observation also implies that shorter GB trajectories may be sufficient to cover the sampling achieved in a longer explicit solvent simulation of the corresponding molecule. These developments point the way to a new generation of simulations for nucleic acids, both at longer time scales and for larger systems, than can reasonably be expected with current explicit solvent methodologies.

Acknowledgment. This work was supported by NIH grant RR12255; V.T. was supported by a pre-doctoral fellowship from the La Jolla Interfaces in Science program. We thank Brian Dominy and Charles Brooks for helpful discussions.

Appendix: Simulation Details

1. Poisson−Boltzmann (PB) Calculations. To obtain the electrostatic component to the solvation free energy using PB, we followed the protocol outlined in Srinivasan et al.[22] using the Delphi-II program. The charges and radii are the same as for the GB calculations. Linear solutions to the PB equations were computed for a solvent dielectric of 78.5, and a solute dielectric of 1, for comparison with GB results.

2. Molecular Dynamics Simulations. The explicit solvent MD simulations with particle mesh Ewald (PME) have all been published elsewhere. These include the A- and B-form DNA d(CCAACGTTGG)$_2$[54] and the A- and B-form RNA r(CCAACGUUGG)$_2$,[53] all using the Cornell et al. force field[48] that forms the gas-phase portion of the present results. For each of the above four simulations, 100 snapshots at 10 ps intervals were used to compare their helical parameters and energy terms with those of GB simulated structures. These are the same structures used by Srinivasan et al.,[22] where a summary and analysis of the simulations can be found.

2.1. A-form r(CCAACGUUGG)$_2$ and B-form d(CCAACGTTGG)$_2$. The starting structures for the GB simulations were first minimized by 100 steps of conjugate gradient minimization. The relaxed structures were then subjected to 40 ps of MD with a 1 fs time-step, gradually heating the structure from 0 to 300 K with 5 kcal/(mol·Å^2) harmonic constraints on the solute to their starting structures, and a time constant for heat bath coupling of 0.8 ps. SHAKE was used[55] to constrain bonds involving hydrogen atoms. This was followed by another 40 ps of MD at 300 K, decreasing the force constant of the harmonic restraints to 1 kcal/(mol·Å^2), then to 0.1 kcal/(mol·Å^2). Finally, 20 ps of fully unconstrained MD was carried out with a temperature coupling constant of 2.0 ps on the solute at 300 K. After these equilibration procedures, the production runs of 2 ns MD

(54) Cheatham, T. E., III; Crowley, M. F.; Fox, T.; Kollman, P. A. *Proc. Natl. Acad. Sci. U.S.A.* **1997**, *94*, 9626−9630.

(55) Ryckaert, J.-P.; Ciccotti, G.; Berendsen, H. J. C. *J. Comput. Phys.* **1977**, *23*, 327−341.

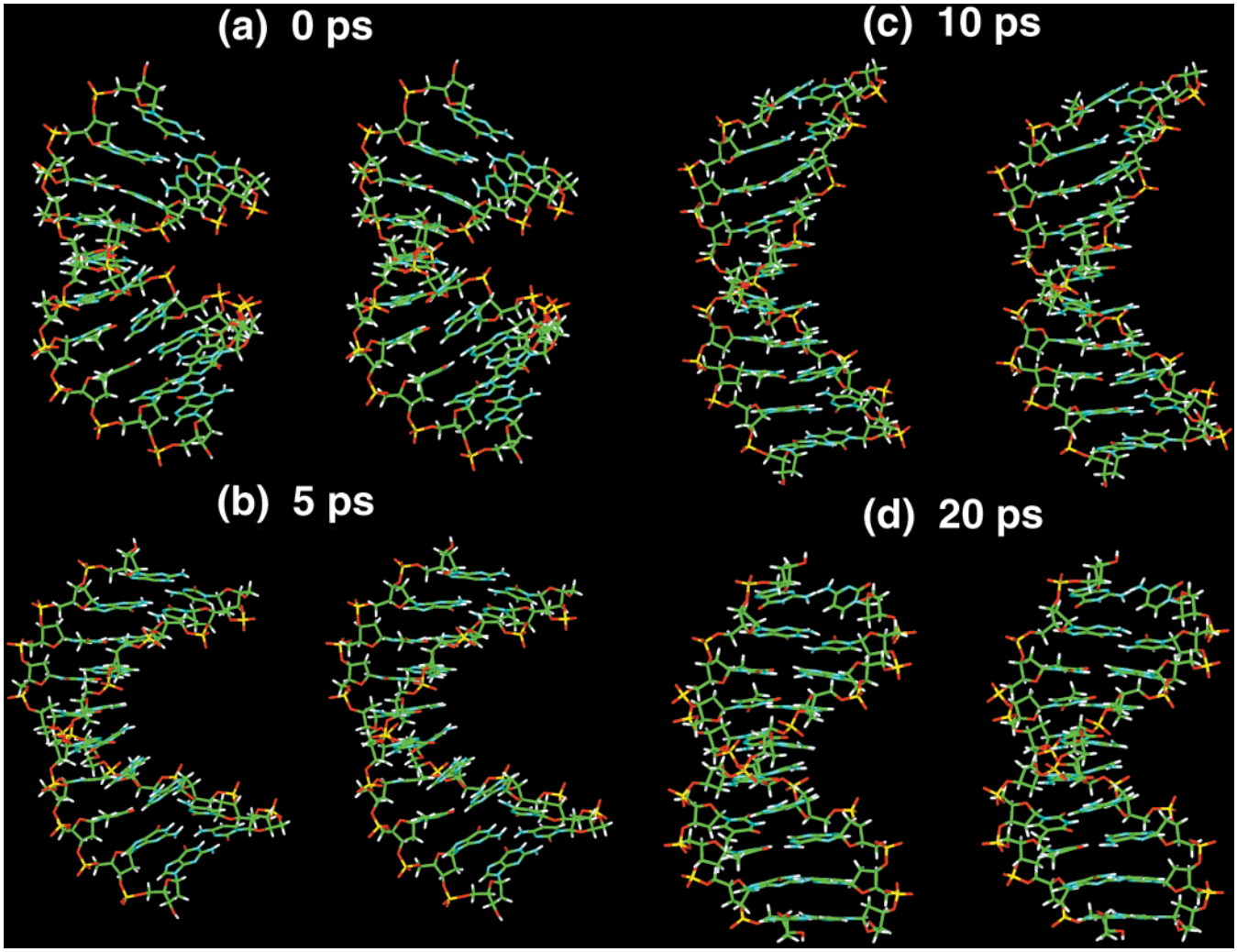

Figure 9. Stereo plots of snapshots at 0, 5, 10, and 20 ps of the unconstrained GB simulation with A-DNA as the starting structure.

Table 6. Timings for 0.1 ps Simulations of d(CCAACGTTGG)$_2$

	no. proc[a]	total (s)[b]	eff.
Vac	2	4.74	1.00
	4	2.50	0.95
	8	1.36	0.87
	16	0.83	0.71
GB	2	30.82	1.00
	4	14.79	1.04
	8	8.24	0.94
	16	4.47	0.86
Wat	2	179.56	1.00
	4	104.43	0.86
	8	56.11	0.80
	16	32.60	0.69

[a] Number of processors of Cray T3E-900. [b] Total non-setup time in seconds.

simulations were performed with constant total energy dynamics. No cutoff of nonbonded interactions was used in these simulations.

2.2. B-form r(CCAACGUUGG)$_2$ and A-form d(CCAACGTTGG)$_2$. These starting structures were taken from snapshots of the explicit solvent simulations of the corresponding nucleic acids. Because the B-form RNA and A-form DNA are not the preferred conformations of these nucleic acids, structural restraints were placed to keep them in these conformations for comparison of energetics.

The structural constraints used to maintain the B-form conformation of the RNA include 58 proton−proton distance restraints and 52 Watson−Crick hydrogen-bonding constraints, with a force constant of 20 kcal/(mol·Å^2). The proton−proton restraints consisted of sequential H1′−H5″, H4′−H5″, H1′−H5, H1′−H6, H1′−H8, H2′−H5, H2′−H6, H3′−H6, H3′−H8, H6−H8, H2−H2, and H8−H8 distances, representing measurable sequential NOEs of B-form nucleic acids,[56] with 0.3 Å plus the internuclear distance measured in a canonical B-form RNA as the upper bound. Because the B-RNA sugar pucker remained in the C2′-endo position within the simulation time, no torsion restraints were added to enforce the sugar conformations.

The structural constraints used to maintain the A-form conformation of the DNA include 44 proton−proton distance restraints, 52 Watson−Crick constraints, and sugar pucker restraints in the form of 100 torsion angle restraints, with a force constant of 20 kcal/(mol·Å^2) on the distance restraints and 20 kcal/(mol·rad^2) on the torsion restraints. The proton−proton restraints consisted of sequential H3′−H5, H1′−H5, H1′−H6, H1′−H8, H2′−H5, H2′−H6, H2−H1′, H3′−H6, H3′−H8, H6−H8, H2−H2, and H8−H8 distances, representing measurable sequential NOEs of A-form nucleic acids,[56] with 0.3 Å plus the internuclear distance measured in a canonical A-form DNA as the upper bound. The sugar puckers were constrained with a lower bound of 0° and an upper bound of 50° using 5 torsion angle restraints (ν_0, ν_1, ν_2, ν_3, ν_4, and ν_5) for each nucleotide.

The equilibration steps were similar to those of the A-RNA and B-DNA simulations, except the distance and torsion restraints were maintained throughout the simulations, and no harmonic constraints were imposed. The starting structures underwent 100 steps of conjugate gradient energy minimization, followed by 40 ps of MD, increasing the temperature from 0 to 300 K. SHAKE was used to constrain bonds involving hydrogen atoms, and the temperature coupling constant was 0.8 ps. This was followed by 20 ps of MD with an increased temperature

(56) Saenger, W. *Principles of nucleic acid structure*; Springer-Verlag: New York, 1984.

coupling constant of 2.0 ps on the solute at 300 K. The production runs of 2 ns MD simulations were performed with a 2.0 ps temperature coupling constant on the solute, rather than at constant total energy, because of the addition of structural restraints.

3. Structural and Energetic Analysis. The helical parameters of RNA and DNA for both static structures and trajectories were analyzed using the Dials and Windows interface to Curves.[57] The minor groove widths were reported as selected inter-strand phosphate distances. Structural parameters for each of the GB trajectories were calculated from 100 snapshots taken at 10 ps intervals for the last nanosecond of the simulations. The explicit solvent structural parameters were calculated from 100 snapshots taken at 10 ps intervals for each simulation, the details of which are summarized in Srinivasan et al.[22] Canonical A- and B-form nucleic acid structures were generated from standard fiber diffraction models.[56]

4. Principal Component Analysis. Quasiharmonic analyses were carried out using *quasih*, a module of AMBER 6, for both the explicit solvent and GB simulations of B-form d(CCAACGTTGG)$_2$. Snapshots of the DNA (not including counterions or water molecules), saved at every 0.2 ps for a total of 1 ns, were superimposed on the inner eight base-pairs. The resulting trajectory was used to compute the matrix of Cartesian fluctuations. Diagonalization of this matrix led to the quasiharmonic frequencies and directions.[51]

JA9939385

(57) Ravishanker, G.; Swaminathan, S.; Beveridge, D. L.; Lavery, R.; Sklenar, H. *J. Biomol. Struct. Dyn.* **1989**, *6*, 669−699.